J|A|C|S
ARTICLES
Published on Web 04/20/2002

Bond Insertion, Complexation, and Penetration Pathways of Vapor-Deposited Aluminum Atoms with HO- and CH_3O-Terminated Organic Monolayers

Gregory L. Fisher,[§] Amy V. Walker,[†] Andrew E. Hooper,[||] Timothy B. Tighe,[†] Kevin B. Bahnck,[⊥] Hope T. Skriba,[†] Michael D. Reinard,[†] Brendan C. Haynie,[†] Robert L. Opila,*[,‡] Nicholas Winograd,*[,†] and David L. Allara*[,†]

Contribution from the Department of Chemistry, The Pennsylvania State University, University Park, Pennsylvania 16802, and Department of Materials Science, University of Delaware, Newark, Delaware 19617

Received October 12, 2001

Abstract: The interaction of vapor-deposited Al atoms with self-assembled monolayers (SAMs) of HS−$(CH_2)_{16}$−X (X = −OH and $-OCH_3$) chemisorbed at polycrystalline Au{111} surfaces was studied using time-of-flight secondary-ion mass spectrometry, X-ray photoelectron spectroscopy, and infrared reflectance spectroscopy. Whereas quantum chemical theory calculations show that Al insertion into the C−C, C−H, C−O, and O−H bonds is favorable energetically, it is observed that deposited Al inserts only with the OH SAM to form an −O−Al−H product. This reaction appears to cease prior to complete −OH consumption, and is followed by formation of a few overlayers of a nonmetallic type of phase and finally deposition of a metallic film. In contrast, for the OCH_3 SAM, the deposited Al atoms partition along two parallel paths: nucleation and growth of an overlayer metal film, and penetration through the OCH_3 SAM to the monolayer/Au interface region. By considering a previous observation that a CH_3 terminal group favors penetration as the dominant initial process, and using theory calculations of Al−molecule interaction energies, we suggest that the competition between the penetration and overlayer film nucleation channels is regulated by small differences in the Al−SAM terminal group interaction energies. These results demonstrate the highly subtle effects of surface structure and composition on the nucleation and growth of metal films on organic surfaces and point to a new perspective on organometallic and metal−solvent interactions.

1. Introduction

The underlying chemistry of the interaction of metal atoms with organic thin films and polymer surfaces has important implications in many areas of science and technology.[1] Elucidation of the fundamental reaction pathways has proven to be particularly challenging over the years since for most organic systems the precise nature of the organic surface is difficult to ascertain. The use of self-assembled monolayers (SAMs),[2−4] which provide a known surface density of uniformly organized organic groups at the vacuum interface, recently has provided an approach to overcoming this problem.[5−16] Not only are SAMs of use as generalized models for metal−organic interactions involving a wide variety of organic surfaces, but they also have become of direct interest recently with the discovery that electronic devices can be fabricated using SAMs with deposited metal contacts. The study of the metal−SAM interactions in

* To whom correspondence should be addressed. E-mail (D.L.A.): dla3@psu.edu.
[†] The Pennsylvania State University.
[‡] University of Delaware.
[§] Present address: Los Alamos National Laboratories, Los Alamos, NM 87545.
[||] Present address: Motorola Corporate Laboratories, Tempe, AZ 85284.
[⊥] Present address: Pfizer Laboratories, Inc., Groton, CT 06340.

(1) For example, see: Mittal, K. L., Ed. *Metallized Plastics 5 & 6: Fundamental and Applied Aspects*; VSP International Science Publishers: The Netherlands, 1998; and earlier volumes. Mittal, K. L., Ed. *Metallized Plastics: Fundamentals and Applications*; Marcel Dekker: New York, 1998.
(2) Ulman, A. *Chem. Rev.* **1996**, *96*, 1533−1554.
(3) Dubois, L. H.; Nuzzo, R. G. *Annu. Rev. Phys. Chem.* **1992**, *43*, 437−463.
(4) Swalen, J. D.; Allara, D. L.; Andrade, J. D.; Chandross, E. A.; Garoff, S.; Israelachvili, J.; McCarthy, T. J.; Murray, R.; Pease, R.; Rabolt, J.; Wynne, K.; Yu, H. *Langmuir* **1987**, *3*, 932−950.
(5) Jung, D. R.; Czanderna, A W. *Crit. Rev. Solid State Mater. Sci.* **1994**, *19*, 1−54.
(6) Jung, D. R.; Czanderna, A. W.; Herdt, G. C. *J. Vac. Sci. Technol.* **1996**, *A14*, 1779−1787.
(7) Czanderna, A. W.; King, D. E.; Spaulding, D. *J. Vac. Sci. Technol.* **1991**, *A9*, 2607−2613.
(8) Jung, D. R.; King, D. E.; Czanderna, A. W. *J. Vac. Sci. Technol.* **1993**, *A11*, 2382−2386.
(9) Konstadinidis, K.; Zhang, P.; Opila, R. L.; Allara, D. L. *Surf. Sci.* **1995**, *338*, 300−312.
(10) Tarlov, M. J. *Langmuir* **1995**, *11*, 80−89.
(11) Dressick, W. J.; Dulcey, C. S.; Georger, J. H., Jr.; Calabrese, G. S.; Calvert, J. M. *J. Electrochem. Soc.* **1994**, *141*, 210−220.
(12) Jung, D. R.; King, D. E.; Czanderna, A. W. *Appl. Surf. Sci.* **1993**, *70/71*, 127−132.
(13) Herdt, G. C.; Czanderna, A. W. *Surf. Sci. Lett.* **1993**, *297*, L109−L112.
(14) Hirose, Y.; Kahn, A.; Aristov, V.; Soukiassian, P. *Appl. Phys. Lett.* **1996**, *68*, 217−219.
(15) Herdt, G. C.; King, D. E.; Czanderna, A. W. *Z. Phys. Chem.* **1997**, *202*, 163−196.
(16) Mittal, K.; Lee, K. W., Eds. *Polymer Surfaces and Interfaces: Characterization, Modification, and Applications*; VSP International Science Publishers: The Netherlands, 1999; pp 189−224.

10.1021/ja0123453 CCC: $22.00

these structures should prove very useful in designing ohmic contacts[17]. Also, from a fundamental perspective, SAMs offer an interesting and useful complement to studies of the solvation and electron-transfer reactions of metal atoms with gas-phase molecules and molecular clusters.[18−20] While the fundamental solvation and chemical interaction mechanisms of a given metal atom−molecule (or molecular group) system are fixed (e.g., electrostatic, van der Waals, electron exchange), variation of the system geometry can vary the degree of the interactions. In particular, with SAMs the interactions are constrained to occur within a quasi-2-D planar geometry, in contrast to the 3-D configurations allowed in a single phase.

Of the various metals to consider, Al has been of particular interest to us because of its common use in metallization of polymers and as top contacts in organic electronic devices.[16,21] Further, in terms of a complement to gas-phase solvation studies, as noted above, there has been interest in characterizing the interaction of Al atoms with clusters of small gas molecules such as H_2O, NH_3, and $(CH_3)_2O$,[22−24] closely analogous to the interaction of Al atoms with terminal SAM groups such as $-NH_2$, $-OH$, and $-OCH_3$.

Recently, we reported on the deposition of Al atoms onto H_3CO_2C- (methyl ester) and H_3C-terminated alkanethiolate/Au{111} SAMs.[25,26] It was observed that Al atoms exhibit an unexpectedly subtle and discriminating chemistry with these monolayers. In both cases, no reaction of the Al occurs with the $-CH_2-$ groups of the alkyl chains. In the case of the $-CH_3$ termination, deposited Al atoms were observed to penetrate through the monolayer to the S/Au interface where it appeared that each Al atom inserted into a Au−S bond to form an aluminum thiolate species. Upon completion of this adlayer, Al was observed to begin depositing exclusively at the vacuum/SAM interface. In the case of the H_3CO_2C-terminated SAM, the deposited Al atoms do not penetrate through the SAM but rather react in a 1:1 stoichiometry with the carbonyl portion of the ester functionality while leaving the C−O (ether) linkage intact. Further, past the first deposited Al atom per group, about four additional Al atoms continue to undergo redox interactions with the terminal group leading to an organo-aluminum complex with nonzero Al valence states. In a subsequent study[27] involving a HO_2C-terminated alkanethiolate/Au{111} SAM, we reported that Al atoms react with the acid group in an ~1:1 average stoichiometry with no penetration into the SAM. An intriguing aspect of this study is that while the chemical degradation of the CO_2H group occurs during the initial deposition of the Al atoms, some 15−20% fail to react, even with continued deposition up to many Al atoms per molecule.

Two main conclusions have emerged from these initial studies. First, when a reactive group is present at the alkyl chain terminus, nucleation and growth of a metallic film occur only at the vacuum/film interface, and the first several layers of Al atoms appear to form an organo-aluminum, dielectric layer prior to the growth of a metallic film. Second, when the chain terminus contains an unreactive CH_3 group, penetration through the SAM to the S/Au interface occurs. It was proposed that this penetration occurs via a thermally activated lateral hopping process of the SAM molecules that leads to the creation of transient holes allowing transport of nearby Al atoms directly to the S/Au interface.[26]

From these studies, the C═O carbonyl oxygen atoms within the $-CO_2CH_3$ and $-CO_2H$ terminal functional groups clearly are implicated as a critical reaction center in the metal−organic interaction. In this paper, we examine this interaction in more detail by studying the interactions of Al atoms with HO- (hydroxy) and H_3CO- (methoxy) terminated alkanethiolates on Au{111}. These functional groups can be viewed simplistically as representing constituents of the $-CO_2CH_3$ group. Studying each constituent thus could be expected to shed light on the subtle preferences of Al for specific molecular reaction sites in this family of O-containing functional groups. In particular, a detailed characterization of the interplay between Al chemical interaction and penetration pathways is critical in establishing a fundamental basis for understanding nucleation and growth processes of Al films on a variety of O-containing organic surfaces.

As in our previous studies, Al deposition was performed at room temperature using thermal sources, and analysis was performed using a combination of in situ surface probes: time-of-flight secondary-ion mass spectrometry (ToF−SIMS), X-ray photoelectron spectroscopy (XPS), and infrared reflection spectroscopy (IRS). In the case of the HO-terminated SAM, our results indicate that Al chemically interacts with the $-OH$ groups yielding products that include an H−Al−O−C structure. Reaction appears to cease after approximately one Al atom is deposited per molecule. The next about four Al atoms per molecule form an electron-deficient (premetallic) overlayer with subsequent deposition forming metallic overlayers. Penetration of the Al atoms to the S/Au interface is not observed. In contrast, when Al is deposited onto a H_3CO-terminated SAM, no chemical reaction with the terminal group is observed; only a weak complexation occurs. Instead, initial deposition of an average of three atoms per molecule results in penetration through the monolayer to the S/Au interface, reminiscent of the behavior of the H_3C-terminated SAM reported previously.[26] Further deposition results in formation of an Al overlayer

(17) For example, see: (a) Tour, J. M. *Acc. Chem. Res.* **2000**, *33*, 791−804. (b) Reed, M. A.; Tour, J. M. *Sci. Am.* **2000**, *282*, 86−93. (c) Metzger, R. M.; Xu, T.; Peterson, I. R. *J. Phys. Chem. B* **2001**, *105*, 7280−7290. (d) Metzger, R. M.; Chen, B.; Hopfner, U.; Lakshmikantham, M. V.; Vuillaume, D.; Kawai, T.; Wu, X. L.; Tachibana, H.; Hughes, T. V.; Sakurai, H.; Baldwin, J. W.; Hosch, C.; Cava, M. P.; Brehmer, L.; Ashwell, G. J. *J. Am. Chem. Soc.* **1997**, *119*, 10455−10466. (e) Collier, C. P.; Wong, E. W.; Belohradsky, M.; Raymo, F. M.; Stoddart, J. F.; Kuekes, P. J.; Williams, R. S.; Heath, J. R. *Science* **1999**, *285*, 391−394. (f) Heath, J. R.; Kuekes, P. J.; Snider, G. S.; Williams, R. S. *Science* **1998**, *280*, 1716−1721.

(18) Duncan, M. A. *Int. J. Mass Spectrom.* **2000**, *200*, 545−569.

(19) Niedner-Schatteburg, G.; Bondybey, V. E. *Chem. Rev.* **2000**, *100*, 4059−4086.

(20) Lisy, J. M. *Int. Rev. Phys. Chem.* **1997**, *16*, 267−289.

(21) For example, see: (a) Beierlein, T. A.; Brutting, W.; Riel, H.; Haskal, E. I.; Muller, P.; Rieb, W. *Synth. Met.* **2000**, *111−112*, 295−297. (b) Campbell, I. H.; Smith, D. L. *Appl. Phys. Lett.* **1999**, *74*, 561−563. (c) Polzonetti, G.; Russo, M. V.; Infante, G.; Furlani, A. *J. Electron Spectrosc. Relat. Phenom.* **1997**, *85*, 73−80. (d) Faraggi, E. Z.; Davidov, D.; Cohen, G.; Noach, S.; Golosovsky, M.; Avny, Y.; Neumann, R.; Lewis, A. *Synth. Met.* **1997**, *85*, 1187−1190. (e) Vuillaume, D.; Boulas, C.; Collet, J.; Davidovotis, J. V.; Rondelez, F. *Appl. Phys. Lett.* **1996**, *69*, 1646−1648. (f) Gupta, R.; Misra, S. C. K.; Malhotra, B. D.; Beladakere, N. N.; Chandra, S. *Appl. Phys. Lett.* **1991**, *58*, 51−52.

(22) Jursic, B. S. *Chem. Phys.* **1998**, *237*, 51−58.

(23) Di Palma, T.; Latini, A.; Satta, M.; Varvesi, M.; Giardini, A. *Chem. Phys. Lett.* **1998**, *284*, 184−190.

(24) Sakai, S. *J. Phys. Chem.* **1993**, *97*, 8917−8921.

(25) Fisher, G. L.; Hooper, A. E.; Opila, R. L.; Jung, D. R.; Allara, D. L.; Winograd, N. *J. Electron Spectrosc. Relat. Phenom.* **1998**, *99*, 139−148.

(26) Hooper, A. E.; Fisher, G. L.; Konstadinidis, K.; Jung, D. R.; Nguyen, H.; Opila, R. L.; Collins, R. W.; Winograd, N.; Allara, D. L. *J. Am. Chem. Soc.* **1999**, *121*, 8052−8064.

(27) Fisher, G. L.; Hooper, A. E.; Opila, R. L.; Allara, D. L.; Winograd, N. *J. Phys. Chem.* **2000**, *104*, 3267−3273.

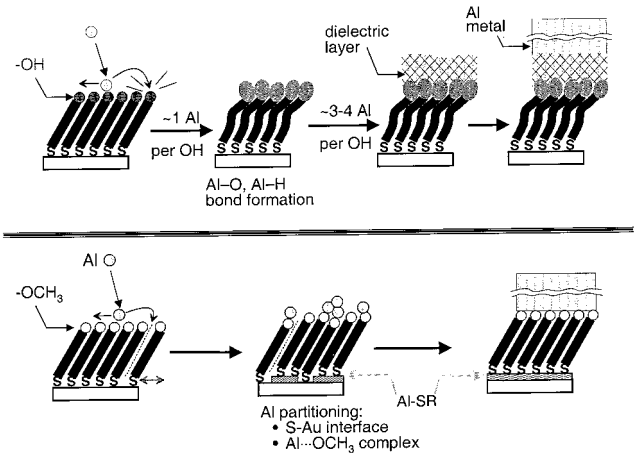

Figure 1. Cartoon illustrations of the important features of the interaction regimes of deposited Al on the HO SAM (top) and the OCH_3 SAM (bottom). The structures depicted are based on common interpretations drawn from the combined ToF−SIMS, XPS, and IR data. The metal overlayer in the diagram of the OCH_3 SAM is sketched arbitrarily as a smooth film for purposes of presentation. The detailed morphology remains to be characterized.

growing from the vacuum/SAM interface. A pictorial summary of the results is shown in Figure 1.

2. Experimental and Methods

2.1. Materials and General Procedures. Ethanol (Pharmco), hexadecanolide (Sigma Aldrich), acetic acid ($^{18}O_2$), and methanol (^{18}O) (Isotec) and all other reagents were used as received, except for THF (Aldrich), which was dried by distillation from Na/benzophenone, and CH_3OH, which was distilled from Mg turnings. All glass apparatus was flame dried and purged with dry N_2. Reactions were performed in a static N_2 atmosphere. Flash column chromatography was performed using 230−400 mesh silica gel, and melting points were taken using a Thomas Hoover melting point apparatus. All ^1H NMR spectra were obtained on a Bruker 200 MHz spectrometer. The aluminum metal for all depositions (Goodfellow and R. D. Mathis) was of ≥99.999% purity.

2.2. SAM Preparation. The preparation and characterization of the types of SAMs used in this study have been described in detail previously.[28,29] The deposition metals (Au and Cr; Goodfellow and R. D. Mathis, respectively; purities ≥99.99%) were thermally deposited sequentially (Cr, ∼5 nm; Au, ∼200 nm) onto clean Si(001) native oxide covered wafers. Self-assembly of well-organized monolayers was achieved by immersing the Au substrates into millimolar solutions of the relevant hexadecanethiol molecules in absolute ethanol for ∼4 days at ambient temperature. The films were characterized with single wavelength ellipsometry, infrared spectroscopy, and contact angle measurements to ensure dense packing and clean surfaces. In addition, all SAMs were characterized by the initial ToF−SIMS, XPS, and IRS measurements prior to metal deposition.

2.3. Time-of-Flight Secondary Ion Mass Spectrometry. The ToF−SIMS analyses were performed on a custom designed instrument, as described previously.[30] Briefly, the instrument consists of a loadlock, a preparation chamber, and the primary analysis chamber, each separated by a gate valve. The primary Ga^+ ions were accelerated to 25 and 15 keV for the HO- and H_3CO-terminated SAM studies, respectively. The ions were contained in a 100 nm diameter beam that was rastered over a 1600 × 1600 μm^2 area during data acquisition. All spectra were acquired using a total ion dose of less than 10^{11} ions/cm^2. Relative peak intensities are reproducible to within ±6% from both sample to sample and scan to scan.

Aluminum was deposited onto the sample at room temperature from a W wire basket source at a rate of ∼0.15 atoms nm^{-2} s^{-1} with the pressure remaining below 5×10^{-8} Torr. After deposition, the forechamber pressure was allowed to recover to the base value of 1.5×10^{-9} Torr before sample transfer to the analysis chamber. The deposited mass/area was monitored using a Maxtek, Inc. TM-400 quartz crystal microbalance (QCM) controller with a maximum error within ±8%.

2.4. X-ray Photoelectron Spectroscopy. The XPS analyses were performed on a spectrometer (Scienta ESCA 300) equipped with a monochromatic Al Kα source, as described in detail elsewhere.[31,32] A pass energy of 75 eV and an energy step of 0.05 eV were used for the analysis. The resulting full width at half maximum (fwhm) for Au $4f_{7/2}$ is 0.52 eV. A binding energy of 84.00 eV for Au $4f_{7/2}$ was used as a reference for all spectra.

Following analysis of the bare monolayer, the sample was transferred under vacuum to the deposition chamber, which is isolated from the analysis chamber by a gate valve. The pressure in the preparation chamber remained below 5×10^{-8} Torr during the deposition. Incremental amounts of Al were deposited at a highly controlled, constant rate, typically near ∼0.1 atoms nm^{-2} s^{-1}, by evaporation from a graphite crucible. The deposition rate was checked periodically by removing a reference sample and analyzing with Rutherford backscattering spectroscopy (RBS). After deposition, the Al/SAM specimen was transferred directly under vacuum to the analysis chamber where the pressure was maintained below 5×10^{-9} Torr.

2.5. Infrared Spectroscopy. Analyses were performed on a Fourier transform instrument (Mattson Research Series 1000) fitted with custom in-house optics configured external to the instrument and designed for grazing incidence reflection of samples under vacuum. A liquid nitrogen cooled MCT detector was used with an effective low-frequency cutoff of ∼750 cm^{-1}. The infrared beam was allowed to access the vacuum system and reflect from the sample through a pair of differentially pumped KBr windows. After analysis of the bare monolayer, a shield was moved to unblock the path between the sample and the Al source. The Al metal was evaporated from a W-wire basket at a rate of ∼0.15 atoms nm^{-2} s^{-1} as measured by a QCM. The pressure remained below 1×10^{-7} Torr during the deposition.

2.6. Quantum Theory Calculations. Density functional theory (DFT) calculations were performed to give estimates of the interaction energies between Al atoms and the various constituent groups of the molecules in the SAMs and to show associated changes in the molecular vibrational spectra. The calculations were done using the algorithms available in the Gaussain 98 program package.[33] The small sytems (less than five heavy atoms) were geometry optimized using the B3PW91 functional with 6-31G(d,p), 6-31+G(d,s), 6-311+G(d,p), and 6-311+G-(2d,fp) basis sets.[34,35] For the larger systems, the B3PW91/6-31G(d,p) level of theory was employed. In all cases, frequency calculations were

(28) Nuzzo, R. G.; Dubois, L. H.; Allara, D. L. *J. Am. Chem. Soc.* **1990**, *112*, 558−569.
(29) Laibinis, P. E.; Bain, C. D.; Nuzzo, R. G.; Whitesides, G. M. *J. Phys. Chem.* **1995**, *99*, 7663−7676.
(30) Braun, R. M.; Blenkinsopp, P.; Mullock, S. J.; Corlett, C.; Willey, K. F.; Vickerman, J. C.; Winograd, N. *Rapid Commun. Mass Spectrom.* **1998**, *12*, 1246−1252.
(31) Beamson, G.; Briggs, D.; Davies, S. F.; Fletcher, I. W.; Cark, D. T.; Howard, J.; Gelius, U.; Wannberg, B.; Balzer, P. *Surf. Interface Anal.* **1990**, *15*, 541−549.
(32) Gelius, U.; Wannberg, B.; Baltzer, P.; Fellnerfeldegg, H.; Carlsson, G.; Johansson, C. G.; Larsson, J.; Munger, P.; Vegerfors, G. *J. Electron Spectrosc. Relat. Phenom.* **1990**, *52*, 747−785.
(33) Frisch, M. J.; Trucks, G. W.; Schlegel, H. B.; Scuseria, G. E.; Robb, M. A.; Cheeseman, J. R.; Zakrzewski, V. G.; Montgomery, J. A., Jr.; Stratmann, R. E.; Burant, J. C.; Dapprich, S.; Millam, J. M.; Daniels, A. D.; Kudin, K. N.; Strain, M. C.; Farkas, O.; Tomasi, J.; Barone, V.; Cossi, M.; Cammi, R.; Mennucci, B.; Pomelli, C.; Adamo, C.; Clifford, S.; Ochterski, J.; Petersson, G. A.; Ayala, P. Y.; Cui, Q.; Morokuma, K.; Malick, D. K.; Rabuck, A. D.; Raghavachari, K.; Foresman, J. B.; Cioslowski, J.; Ortiz, J. V.; Stefanov, B. B.; Liu, G.; Liashenko, A.; Piskorz, P.; Komaromi, I.; Gomperts, R.; Martin, R. L.; Fox, D. J.; Keith, T.; Al-Laham, M. A.; Peng, C. Y.; Nanayakkara, A.; Gonzalez, C.; Challacombe, M.; Gill, P. M. W.; Johnson, B. G.; Chen, W.; Wong, M. W.; Andres, J. L.; Head-Gordon, M.; Replogle, E. S.; Pople, J. A. *Gaussian 98*, revision A.9; Gaussian, Inc.: Pittsburgh, PA, 1998.

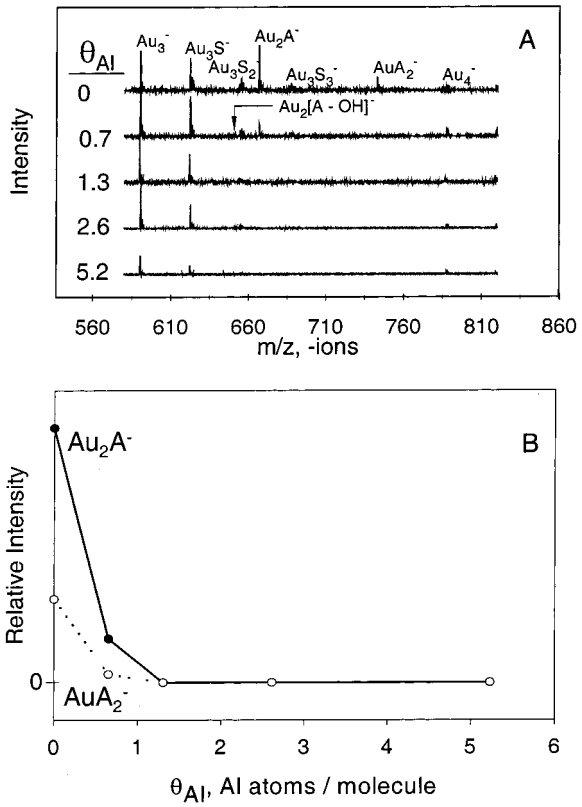

Figure 2. (A) Negative SIMS spectra showing the 580−820 *m*/*z* region of the OH SAM prior to and following deposition of Al. (B) Integrated peak area of Au_2A^- and AuA_2^- plotted versus θ_{Al}.

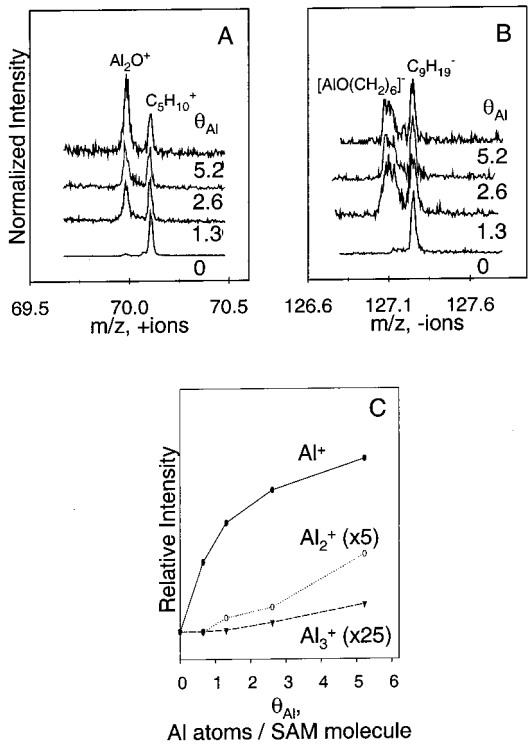

Figure 3. High-resolution SIMS spectral overlays from the OH SAM. The spectra show the evolution of metal-organic fragment ions with Al deposition. (A) Positive ions, nominal mass 70 amu. (B) Negative ions, nominal mass 127 amu. The spectra are normalized to the initial peak intensities of $C_5H_{10}^+$ and $C_9H_{19}^-$, respectively. (C) Integrated peak areas of Al^+, Al_2^+, and Al_3^+ plotted versus θ_{Al}.

performed to ensure the geometry was a true minimum. As a cross check, we note that our levels of theory give results that compare closely with the reported results of MP4(SDTQ), MP2, QCISD, and CCSD-(T) calculations of the energetics of Al−H_2O complexes.[24,36]

At least 20 calculations were done for each level of theory to test the reproducibility of the energies, and several starting geometries for all the different levels of theory were used to ensure geometry convergence. To put the results on a more thermodynamic basis, the energies are reported as enthalpies of the final structures relative to the isolated reactants and contain zero-point energy corrections and thermal energy corrections for standard conditions of 1 bar and 298 K. The thermal corrections to the zero-point energies are in the range of ∼5 kJ/mol.

3. Results

3.1. Definition of Deposited Al Coverage. The deposition of Al onto the samples was followed directly as the mass per unit area by either QCM or the integrated flux from a controlled rate source (XPS case). For convenience in interpretation of the data, the deposited amounts were converted to coverage in atoms of Al per SAM molecule, designated θ_{Al}, on the basis that there are 4.6 molecules/nm^2 in a well-formed alkanethiolate/Au{111} SAM.[3] Thus for $\theta_{Al} = 1.0$, there would be one Al atom deposited on average per SAM molecule.

3.2. Hydroxyl-Terminated Monolayer. 3.2.1. ToF−SIMS. Negative ions in the mass range from 580 to 820 Da are shown in Figure 2A. With the deposition of Al, there are significant changes in the spectra indicating that a reaction occurs between the Al and the OH group. The areas of the Au_2A^- and AuA_2^- peaks, involving intact adsorbate molecules, are plotted versus θ_{Al} in Figure 2B. The disappearance of these ions with increasing θ_{Al} is a direct indication of the conversion of the original adsorbates to some different chemical structure by the Al atoms. The decrease in the Au_2A^- and AuA_2^- intensities also suggests that on average approximately one Al atom per molecule is required.

Evidence that the changes in the adsorbate structures involve reaction of the OH group with Al to form an Al−O bond can be deduced from the observation of the formation of AlO-containing ions. Two of these ions are shown in Figure 3A,B, where the intensities have been normalized to the initial peak intensities of $C_5H_{10}^+$ and $C_9H_{19}^-$ to make obvious the increasing intensity of the metal-organic fragments with respect to the simple hydrocarbon fragments as the deposition progresses. The appearance of the $[(CH_2)_6OAl]^-$ ion fragment (Figure 3B) indicates that the Al + −OH reaction forms an Al−OR moiety, where R = alkyl. We note that the absolute peak intensities of both the metal-organic and the hydrocarbon fragments reach a maximum intensity at $\theta_{Al} \approx 2-3$ atoms/molecule and then begin to decrease in intensity with increasing deposition (data not shown). This observation is consistent with a uniformly distributed aluminum overlayer. The observation of Al_2O^+ (Figure 3B), again indicative of an Al−OR bond in the reacted

(34) (a) Becke, A. D. *J. Chem. Phys.* **1993**, *98*, 5648−5652. (b) Perdew, J. P. In *Electronic Structure of Solids*; Ziesche, P., Eschrig, H., Eds.; Akademie Verlag: Berlin, 1991; pp 11−20. (c) Perdew, J. P.; Chevary, J. A.; Vosko, S. H.; Jackson, K. A.; Pederson, M. R.; Singh, D. J.; Fiolhais, C. *Phys. Rev. B* **1992**, *46*, 6671−6687.
(35) (a) Wachters, A. J. H. *J. Chem. Phys.* **1970**, *52*, 1033−1036. (b) Hay, P. J. *J. Chem. Phys.* **1977**, *66*, 4377−4384. (c) Raghavachari, K.; Trucks, G. W. *J. Chem. Phys.* **1989**, *91*, 1062−1065.
(36) Fangstrom, T.; Lunell, S.; Kasai, P. H.; Eriksson, L. A. *J. Phys. Chem. A* **1998**, *102*, 1005−1017.

adsorbate species, is interesting since fragments of this type have not been observed in related systems studied to date.[25−27]

To establish unambiguously that the appearance of the Al−O species arises from Al + OH species and not due to reactions with adventitious sources of oxygen, such as H_2O or O_2, further analyses were carried out using $H^{18}O$-terminated SAMS.[37] These data confirm that the deposited Al chemisorbs to the SAM; signals such as $Al_2{}^{18}O^+$ are observed.

Other metal-organic ions observed in the mass spectra after Al deposition are AlO^-, $AlOC^+$, $AlO(CH_2)_x^{\pm}$, and $AlO(CH)_x(CH_2)_y^{\pm}$. Of particular interest is the appearance of $[Au_2S(CH_2)_{16}]^-$ and $[Au_2S(CH_2)_{16}OAl]^-$ ions at nominal masses of 650 and 693, respectively. These data again indicate that the Al + OH group reaction results in the formation of Al−OR bonds. We note that the signal at $m/z = 650$, a non-O-containing fragment, is quite strong in contrast to the O-containing fragment signals at $m/z = 693$ and 70 (Al_2O^+ peak in Figure 3B). These data might suggest that the C−O adsorbate bond is weakened following attachment of the Al.

Evidence that the Al atoms are localized at the top (vacuum interface) of the SAM, in contrast to penetrating into the molecular matrix, is shown directly by the absence of $Au_XAl_YS_Z^-$, AlS_X^-, and $AlS(CH_2)_X^+$ species in the spectra. We have shown previously for ω-substituted hexadecanethiolate SAMs/Au that such peaks involving the combinations of Al with S and Au arise only when the Al penetrates to the S/Au interface, or at least to a location within ~0.5−1 nm of the interface.[25−27]

The lack of penetration as well as the direct formation of a Al−OR species are confirmed by the trends in the intensities of Al^+, Al_2^+, and Al_3^+ peaks with Al coverage, shown in Figure 3C. We have shown previously[25−27] that these signal intensities differ significantly between cases where deposited Al atoms penetrate to the SAM/Au interface (H_3C-terminated) and where they chemisorb at the vacuum/SAM interface (H_3CO_2C- or HO_2C-terminated). For example, when Al is deposited onto the H_3CO_2C-terminated SAM, only Al^+ is observed below $\theta_{Al} \approx 1$, an indication that the overlayer consists primarily of isolated Al atoms bonded to organic functional groups. Appreciable levels of Al_2^+ and Al_3^+ are observed only upon further Al deposition (note the expanded scales in the plots). The appearance of these peaks indicates that reactive sites at the organic monolayer terminus have been depleted, allowing the Al atoms to initiate clustering.[38] The Al_X^+ signals in Figure 3C are similar to those reported for Al deposited onto a H_3CO_2C-terminated monolayer (comparison not shown).[25−27] Note that the Al^+ signal in Figure 3C dominates at $\theta_{Al} \approx 1$, while appreciable levels of Al_2^+ and Al_3^+ appear only at higher coverages. Furthermore, the appearance of Al_2^+ and Al_3^+ in the mass spectrum does not occur until after $\theta_{Al} > 1$. We conclude from these data that approximately one Al atom is bound per hydroxyl functional group. Indeed, the stoichiometry of Al to hydroxyl groups, as indicated by the Al_X^+ cluster data, is in agreement with that of Figure 2B ($Au_XA_Y^-$ vs θ_{Al}).

3.2.2. XPS. The C 1s, O 1s, and Al 2p spectra of the HO SAM, before and after deposition of Al, are shown in Figure 4. A 10° takeoff angle (near grazing) was used to enhance the surface selectivity. The binding energies (BEs) were set relative to the Au $4f_{7/2}$ energy at 84.0 eV.

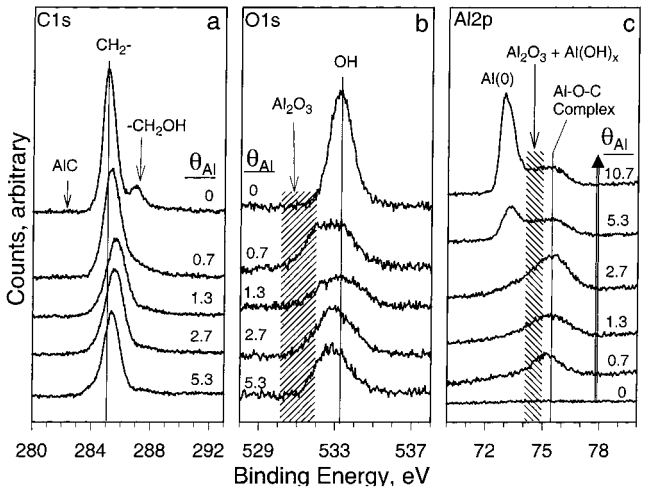

Figure 4. The core-level XPS spectra of the OH SAM prior to and following deposition of Al. A, B, and C represent the C 1s, O 1s, and Al 2p spectra, respectively.

The C 1s spectra of the bare monolayer show peaks at 285.2 and 287.0 eV corresponding to $-\underline{C}H_2-$ and $-\underline{C}H_2OH$, respectively (Figure 4A). A single O 1s peak at 533.4 eV is assigned to the $-CH_2\underline{O}H$ functional group oxygen (Figure 4B). The BEs of these assignments are close to those reported for poly(vinyl alcohol) films.[39]

The spectra are noticeably altered upon deposition of Al. The $-\underline{C}H_2OH$ C 1s peak in Figure 4A is barely observed as a broadening of the high BE side of the $-\underline{C}H_2-$ peak at $\theta_{Al} = 0.7$ Al atoms/molecule and has vanished by $\theta_{Al} < 1.3$. With increasing deposition, the main $-\underline{C}H_2-$ C 1s peak shifts slightly to higher BE (285.7 eV), accompanied by a decrease in signal, then shifts partially back toward the original value. The initial shift can be associated with a lowering of the electron density on the $-\underline{C}H_2-O$ carbon,[40] while intensity attenuation is expected from inelastic photoelectron electron scattering in the Al overlayer. In addition, at low coverages, contributing effects due to the presence of isolated Al atoms or clusters may arise.[41] The lack of a peak in the region around 282 eV where metal carbide species have been reported to appear[9,42,43] is taken as evidence for the absence of formation of Al−C bonds, consistent with our earlier results with other SAMs.[25−27]

Examination of Figure 4B shows that the O 1s peak, initially at 533.4 eV, shifts slightly lower to 532.6 eV and broadens significantly early in the Al deposition. The BE shift indicates an increased electron density on the hydroxyl group O atom, while the broadening suggests the presence of two oxygen species that are close in energy.[40] When $\theta_{Al} > 1.3$, the O 1s peak narrows and shifts to 532.8 eV, a value still lower than

(37) A detailed discussion of the isotope labeling experiments is given in the Supporting Information.
(38) Sigmund, P., Ed. *Fundamental Processes in Sputtering of Atoms and Molecules (SPUT92)*; Bianco Lunos Bogtrykkeri: Denmark, 1992; pp 223−254.
(39) Beamson, G.; Briggs, D. *High-Resolution XPS of Organic Polymers: The Scienta ESCA Database*; John Wiley and Sons: New York, 1992; p 94.
(40) Chakraborty, A K.; Davis, H. T.; Tirrell, M. *J. Polym. Sci., Part A: Polym. Chem.* **1990**, *28*, 3185−3219.
(41) In the low Al atom coverage region, the behavior of the spectra may be influenced by final state effects arising from the presence of isolated Al atoms and small clusters. While these effects constrain the comparisons of the BE values of new peaks with standard assignments to be somewhat qualitative, the internal trends in the observed spectra should remain quite valid.
(42) Akhter, S.; Zhou, X. L.; White, J. M. *Appl. Surf. Sci.* **1989**, *37*, 201−216.
(43) Zhang, P. Study of the Chemistry and Morphology at the Interface between Metals and Polymers by Spectroscopic Techniques. Ph.D. Thesis, Penn State University, 1993.

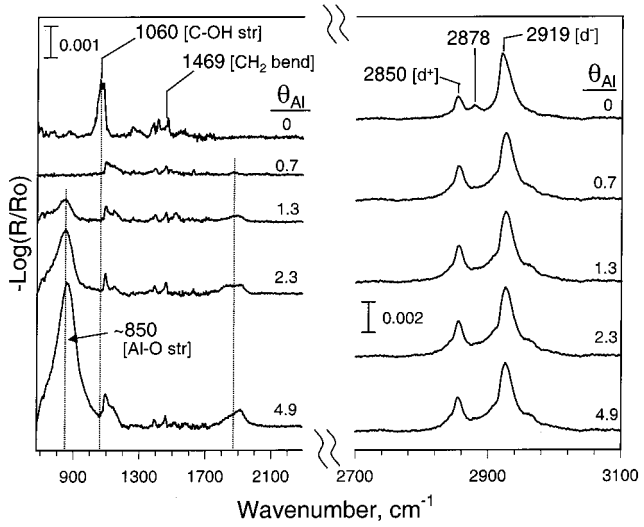

Figure 5. Low- and high-frequency region IRS spectra of the OH SAM prior to and following deposition of Al. Dashed lines are meant to guide the eye to follow the evolution of features attributed to the formation of Al−O and Al−H bonds.

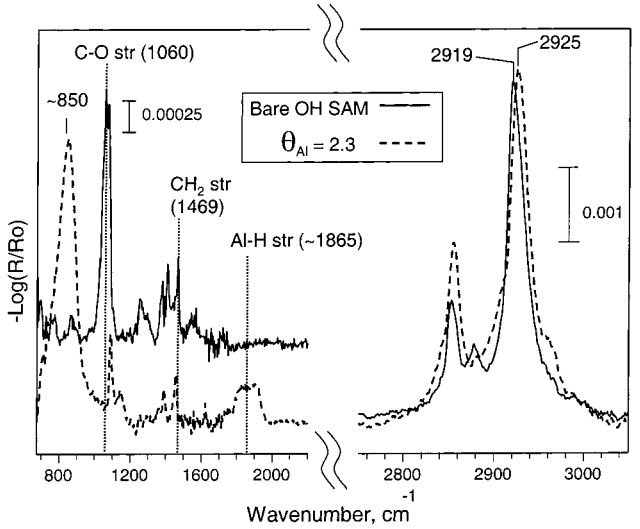

Figure 6. Overlay of the IRS spectra of the bare OH SAM and the same region of the spectrum deposition of Al to a coverage of $\theta_{Al} = 2.3$.

the original one for −OH. This would be consistent with formation of an Al−O bond. Taken together, the C 1s and the O 1s data suggest that O atoms of the OH functional groups react with deposited Al to form an Al−O−C complex with an approximate average stoichiometry of 1:1.[40,44]

The Al 2p spectra in Figure 4C show a peak centered at 75.2 eV when $\theta_{Al} \leq 0.7$. The location of this peak, ~1 eV and ~1.5 to 2.0 eV higher than expected for Al_2S_3 and for Al_2O_3 and $Al(OH)_X$, respectively, suggests the formation of a new Al species. The most likely possibility is an organo-aluminum species formed by reaction with the OH group. When $\theta_{Al} \geq 5.3$, another peak appears at 72.9 eV, corresponding to metallic Al. An intermediate phase with a BE of ~73.5 eV exists between chemisorption of initially deposited Al ($\theta_{Al} \lesssim 0.7$) and formation of a metallic overlayer ($\theta_{Al} \gtrsim 5.3$). This phase is apparently nonmetallic as evidenced by the fact that the metallic Al peak is located 0.6 eV lower in binding energy.[25−27,42,44]

The overall analysis of the data[41] indicates that as the deposition progresses Al atoms first bind with the oxygen of the OH groups to form an ~1:1 Al−O−C organometallic species. Following this, about four more Al atoms deposit to give a phase with nonmetallic character followed finally at higher coverages by the formation of a metallic Al overlayer.

3.2.3. IRS. The IR spectra of the HO-terminated monolayer, before and after Al deposition, are shown in Figure 5. The peak assignments of the bare monolayer have been reported previously,[28] and the important features are summarized here for ease of comparison: 1060 cm^{-1}, C−O stretch (ν_{C-O}); 1469 cm^{-1}, $-CH_2-$ scissor deformation (γ_{CH2}); 2850 and 2919 cm^{-1}, C−H symmetric (d^+) and antisymmetric (d^-) stretches of the $-CH_2-$ chain, respectively. These data indicate that the starting monolayer is well organized with the alkyl chains primarily in the all-*trans* conformation.[28] Other small features in the low-frequency region between the 1060 and 1469 peaks were not interpreted since the signal level was too close to the noise limit for useful analysis. The small absorption at 2878 cm^{-1} is assigned as a stretching mode that is unique to the hydroxyl-terminated monolayer and which is proposed to be associated with the HO− group mediated conformation of the terminal $-CH_2-$ unit on the alkyl chain.[28]

The features related to the OH group are significantly perturbed upon deposition of Al. In particular, the 1060 cm^{-1} C−O stretching mode peak disappears by $\theta_{Al} \lesssim 0.7$, while a new sharp feature appears at 1095 cm^{-1}. The changes can be seen in more detail in Figure 6, which shows an overlay of the initial spectrum and one after $\theta_{Al} = 2.3$.

Because the 1095 cm^{-1} feature arises in the general C−O stretching mode region, it is likely that the C−O bond has not been broken but only perturbed, for example, by Al insertion into the O−H bond to form a C−O−Al−H species. Aluminum alkoxides generally have C−O stretching modes in the region of 1000−1100 cm^{-1}; for example, $Al(OC_2H_5)_3$ exhibits a strong C−O stretching mode peak at 1059 cm^{-1}.[45,46]

As the deposition progresses, the lack of changes in this new band indicates that no further reaction with the −OH group occurs. In contrast to the C−O stretching mode behavior, the CH_2 bending mode is relatively unaffected by Al deposition.

Note the very strong, broad (fwhm ≈ 200 cm^{-1}) feature centered at ~850 cm^{-1} that appears when $\theta_{Al} \gtrsim 1.3$ and intensifies as coverage increases. This band position is typical of Al−O stretching modes, for example, as seen in the LO mode of Al_2O_3[47] and is tentatively assigned to an Al−O species resulting from reaction of Al with the OH group.[48]

Appearing in concert with the ~850 cm^{-1} peak is a broad (fwhm = 125 cm^{-1}) peak at ~1865 cm^{-1}. The possibility of an overtone of the fundamental Al−O absorption is excluded since that should appear at ~1700 cm^{-1}, ~150 cm^{-1} lower in frequency than the observed band. The feature, however, does fall in the range for an Al−H stretching mode. Typical values for various organoaluminum hydrides are observed between 1675 and 1925 cm^{-1} with compounds of the general type HAl(R)(OR′) exhibiting peaks in the 1800−1850 cm^{-1} region.[45,46]

(44) Stoyanov, P.; Akhter, S.; White, J. M. *Surf. Interface Anal.* **1990**, *15*, 509−515.
(45) Maslowski, E., Jr. *Vibrational Spectra of Organometallic Compounds*; Wiley: New York, 1977; pp 107−134.
(46) Compton, T. R. *Comprehensive Organometallic Analysis*; Plenum: New York, 1987; pp 283−308.
(47) Mertens, F. P. *Surf. Sci.* **1978**, *71*, 161−173.

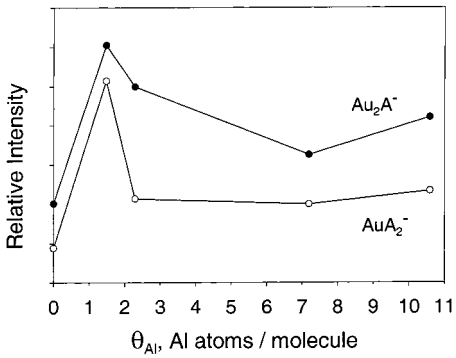

Figure 7. Integrated SIMS peak areas of Au_2A^- and AuA_2^- plotted versus θ_{Al} for the OCH_3 SAM.

We note though that these bands are typically much narrower than the observed 1865 cm^{-1} feature. This indicates significant inhomogeneous broadening in the stretching mode of the surface compounds relative to pure organoaluminum compounds. Steric crowding of the relatively large organo-aluminum species formed at the monolayer termini would be expected to lead to a distribution of molecular configurations that would give rise to inhomogeneous broadening. Such effects also seem likely as interpreted from the C−H stretching mode changes noted below.

The high-frequency region of the spectrum indicates that the symmetric and antisymmetric C−H stretches shift to higher frequency and broaden by $\theta_{Al} \approx 1.3$ Al atoms/molecule with the d^- mode shifted upward by 6 cm^{-1} at $\theta_{Al} \approx 2.3$. These results indicate that the conformational ordering of the alkyl chains decreases when Al is deposited. This effect is expected on the basis that steric crowding of the organo-aluminum species would disrupt chain packing via creation of gauche disorder which would propagate down the chains away from their termini.[25−27]

3.3. Methoxy-Terminated Monolayer. 3.3.1. ToF−SIMS. After deposition of Al, an important diagnostic feature in the ToF−SIMS spectra, shown in Figure 7, is the relatively constant intensity of the Au_2A^- and AuA_2^- peaks, which involve intact adsorbate molecules. Note in Figure 7 how the areas of these peaks barely drop below their initial values in the bare SAM at continued Al deposition. These data indicate that deposition of Al leaves the adsorbate molecule chemically intact. Thus there is no reaction between the Al atoms and the OCH_3 groups. Consistent with this interpretation, the hydrocarbon fragment peak intensities remain relatively unchanged during the early stages of the deposition (data not shown). Upon deposition of the first increment of Al, the increase of the Au_2A^- and AuA_2^- peak intensities (Figure 7) is ascribed to electron transfer from electropositive Al atoms to the more electronegative Au atoms and clusters leaving the surface. As the deposition progresses, all peak intensities become increasingly attenuated, consistent with a growing Al overlayer that can block substrate ion ejection.

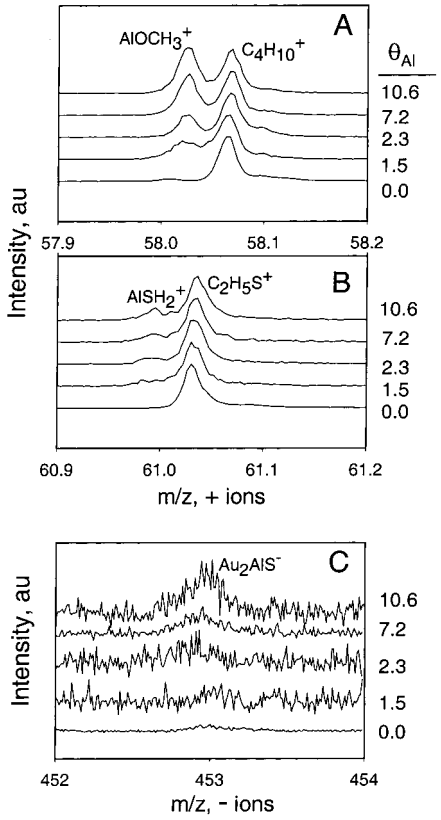

Figure 8. High-resolution SIMS spectral overlays from the OCH_3 SAM. The spectra show the progression of metal-organic fragments with Al deposition. A, B, and C represent, respectively: positive ions, nominal mass 58 Da; positive ions, nominal mass 61 Da; and negative ions, nominal mass 453 Da. The intensities in plots A and B are normalized to the initial peak intensity of $C_4H_{10}^+$ and $C_2H_5S^+$, respectively, whereas the spectra in C are normalized to the peak intensities of Au^-.

In the positive ion mass spectrum, there is evidence that Al interacts with the terminal $-OCH_3$ group. In Figure 8A, the intensity of the $AlOCH_3^+$ ($m/z = 58$) peak is shown for increasing values of θ_{Al}. The spectra are normalized to the initial peak intensities of $C_4H_{10}^+$ to make obvious the changing intensities of the peaks with respect to the hydrocarbon and substrate fragments as the deposition progresses. No $Al_XO_Y^{\pm}$ ions were observed. On the basis of our previous work with $-CO_2H$[27] and $-CO_2CH_3$,[25−27] the appearance of $AlOCH_3^+$ ions but not $Al_XO_Y^{\pm}$ ions indicates that the deposited Al has not undergone an insertion interaction with $-OCH_3$ to form Al−O bonds, and suggests that a weak organo-aluminum complex has formed. This is also consistent with the observed behavior of the AuA_2^- and Au_2A^- ions, which indicates that there is no reaction between the terminal group and Al.

Furthermore, there is also evidence for the simultaneous penetration of the Al atoms to the S/Au interface. In Figure 8B and C, the intensities of the $AlSH_2^+$ ($m/z = 61$) and the Au_2AlS^- ($m/z = 453$) cluster peaks are shown for increasing Al deposition. The spectra are normalized, respectively, to the initial peak intensities of $C_2H_5S^+$ and Au^- to make obvious the

(48) There has been significant controversy over exact assignments of the positions of Al−OC stretching modes in aluminum alkoxides [ref 46] with frequencies ranging from ~500 to 1000 cm^{-1}. The assignments have been complicated in some cases by the presence of Al−O−Al species with associated Al−O stretching modes. At $\theta \approx 1$, the band is taken as evidence for formation of an Al−O bond involving the OH group. While the Al−O stretching cross section is known to be generally intense, for example, in the case of the Al_2O_3 phonon [ref 47], we note that the intensity of our observed mode at higher coverages is considerably stronger than would be expected from comparison to a similarly assigned Al−O stretching mode features in previous studies of Al deposition on HO_2C- and H_3CO_2C-terminated alkanethiolate SAMs on Au [refs 26, 27]. The formation of Al_2O_3 by reaction of Al with adventitious O_2 is not the cause based on ^{18}OH ToF−SIMS data (see Supporting Information). Furthermore, under the identical experimental conditions, Al deposition on other SAMs does not give rise to the intense 850 cm^{-1} feature [refs 25−27]. One possibility for these intensity variations would be variations of the oscillator orientations in the different cases in which the intensity would increase with increasing vertical orientation of the transition dipole.

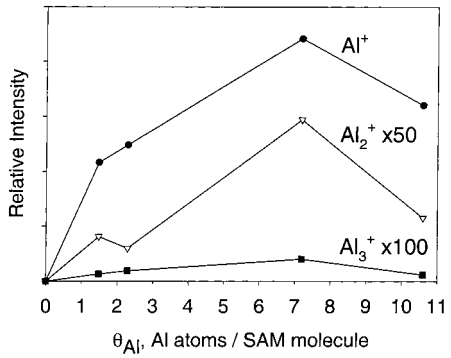

Figure 9. Integrated SIMS ion peak areas of plotted Al_n^+, $n = 1-3$ versus θ_{Al} for the OCH_3 SAM.

changing intensities of the peaks with respect to the hydrocarbon and substrate fragments as the deposition progresses. From our earlier work with the H_3C-terminated SAM,[25,26] the observation of ions containing a combination of Al and S and/or Au indicates that the deposited Al has penetrated through the CH_3O-terminated SAM to the S/Au interfacial region, where the formation of mixed cluster peaks becomes possible (see earlier discussion in section 3.3.1). The intensity of the $AlSH_2^+$ peaks is lower than expected if all the deposited Al penetrated through the SAM to the Au/S interface when compared to our observations of Al deposited on an H_3C-terminated SAM. This reduced intensity is consistent with the deposited Al both penetrating to the Au/S interface and simultaneously associating with the OCH_3 group. We also note that the increasing relative Au_2AlS^- intensity (Figure 8C) throughout the deposition regime suggests that Al penetrates through the SAM to the Au/S interface at all coverages.

Information on the state of the penetrated Al atoms can be seen by examining the Al_X^+ ion signals, shown in Figure 9. These data show that with the first increment of deposited Al, the monomer, dimer, and trimer intensities increase proportionately. We have demonstrated earlier that these signals differ between the case where deposited Al chemisorbs at the monolayer terminus and where it penetrates through the monolayer to the S/Au interface.[25-27] When Al is first deposited onto a H_3C-terminated SAM, which allows penetration, the Al^+ and Al_2^+ increase steadily, whereas there is a slight delay in the Al_3^+ ion. This trend is similar to that for Al deposited onto a bare, clean Au substrate, consistent with the conclusion that the H_3C-terminated SAM allows Al to penetrate completely through the monolayer. In contrast with a reactive terminal group, such as CO_2CH_3[26] or OH (section 3.2.1), when the first increments of Al are deposited on the monolayer, where it chemisorbs, there is an increase in the Al^+ intensity, while there is a slight delay in the Al_2^+ and Al_3^+ that rise in tandem (e.g., see Figure 3C). The early growth of Al_2^+ intensity supports the conclusion that Al penetrates through the OCH_3 SAM to the Au/S interface.

Thus, the OCH_3 SAM appears to exhibit intermediate reactivity to Al when compared to the CH_3 SAM, where Al penetrates through the layer, and the CO_2CH_3, COOH, and OH SAMs, where Al chemisorbs at the SAM terminus group. The absence of $Al_XO_Y^{\pm}$ ions, in contrast to the case of the OH SAM, establishes that Al−O bonds do not form, even at high Al coverage where deposition is at the vacuum/SAM interface. However, the formation of $AlOCH_3^+$ ions (Figure 8A) indicates

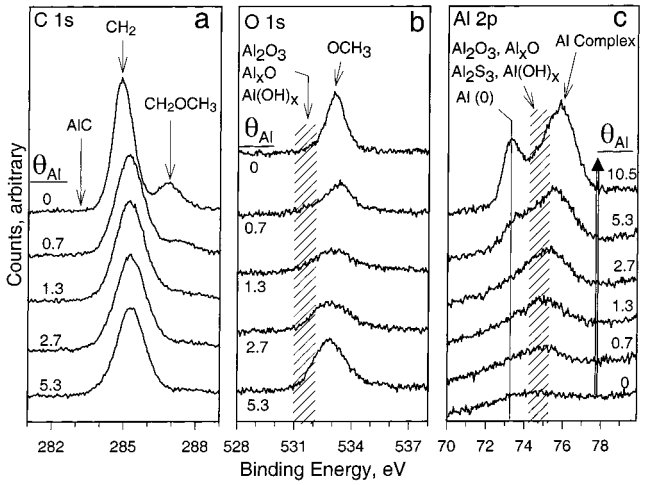

Figure 10. The core-level XPS spectra of the OCH_3 SAM prior to and following deposition of Al. Plots A, B, and C represent the C 1s, O 1s, and Al 2p spectra, respectively.

that an organo-aluminum complex is formed between the terminal group and deposited Al at all coverages. At the same time, we observe the formation of cluster ions between Al and S and/or Au indicating that the deposited is simultaneously penetrating to the Au/S interface.

3.3.2. XPS. The C 1s, O 1s, and Al 2p core-level shifts for the H_3CO-terminated SAM are shown in Figure 10. The data were collected under similar conditions to that of the HO-terminated SAM, except that a 15° takeoff angle was used instead of 10°. The C 1s spectra peaks at 284.9 and 286.8 eV are ascribed to the $-(\underline{C}H_2)-$ alkyl chain and the $-\underline{C}H_2OCH_3$ C atoms, respectively (Figure 10A). The single O 1s peak at 533.1 eV is assigned to $-CH_2\underline{O}CH_3$ (Figure 10B). These assignments are in good agreement with those reported for poly(vinyl methyl ether).[49]

The absence of any features near 282 eV indicates that no aluminum carbide species form.[9,42,43] The vanishing of the $-CH_2OCH_3$ C 1s peak, at 286.8 eV (Figure 10A), by $\theta_{Al} < 1.3$ Al atoms/molecule indicates an ∼1:1 perturbing interaction between Al and the SAM that lowers these BEs, merging them into the main $-CH_2-$ peak. In turn, the $-\underline{C}H_2-$ C 1s peak broadens and shifts to slightly higher binding energy (285.3 eV) as the deposition progresses.[41]

During the initial stages of Al deposition, the 533.1 eV O 1s peak broadens and loses intensity, while a second peak at 532.5 eV appears and increases in intensity. By $\theta_{Al} \approx 5.3$ atoms/molecule, the two peaks combine into one broad peak centered at 532.8 eV. Together with the C 1s data, this indicates that the Al atoms interact with the O atoms of the OCH_3. Further analysis is complicated by the formation of what appears to be an aluminum oxide species, presumably caused by reaction with O_2 and/or H_2O background gases.[50]

The Al 2p spectra show the appearance at the higher coverages of two peaks centered at 75.2 and ∼74 eV. The latter is close to one observed in our previous work on the H_3C-terminated SAM[26] and would be consistent with an Al−S species. This assignment in the present case is supported by

(49) Beamson, G.; Briggs, D. *High-Resolution XPS of Organic Polymers: The Scienta ESCA Database*; John Wiley and Sons: New York, 1992; p 90.
(50) By the time these high coverages are delivered in the XPS experiments, the samples have been exposed for much longer times than in the ToF−SIMS and IRS experiments (∼10 h vs 1 h).

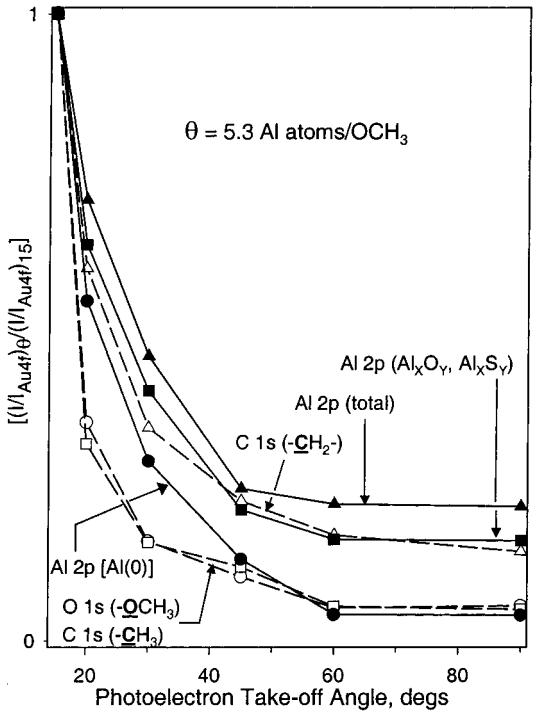

Figure 11. Plots of the XPS peak intensities versus the photoelectron takeoff angle for the OCH_3 SAM before and after Al deposition to a coverage of $\theta_{Al} = 5.3$. A normalized intensity is plotted as defined by $(I/I_{Au4f})_\theta/(I/I_{Au4f})_{15}$, where I and I_{Au4f}, respectively, are the selected core-level intensity and the corresponding Au 4f peak intensity for the same spectral acquisition. The term $(I/I_{Au4f})_\theta$ represents the ratio for a spectra recorded at the takeoff angle of interest, and $(I/I_{Au4f})_{15}$ represents the ratio for spectra taken at 15°. Spectra were taken for O 1s, -OCH_3 (○); C 1s, $-OCH_3$ (□); C 1s, $-CH_2-$ (△); Al 2p, Al (metallic) (●); Al 2p, ($Al_XO_Y + Al_XS_Y$) (■); Al 2p, total Al intensity from all peaks (▲). For details see text.

the ToF−SIMS data (see section 3.2.1) that show that some fraction of the deposited Al atoms penetrates to the S/Au interface. The peak observed at 75.2 eV is at a higher energy than that expected for aluminum oxide. In our previous studies, a peak at this energy was assigned to Al interacting with an O of $-CO_2H$ and $-CO_2CH_3$ groups.[25,26] By analogy, we assign the peak to be associated with Al coordinated with the OCH_3 group in some fashion.

Both the 74.2 and the 75.2 eV peaks continue to grow in intensity until $\theta_{Al} \approx 2.7$. At this point, the 74.2 eV peak starts to attenuate with further Al deposition, while the first signs of metallic Al arise at 72.9 eV. Further analysis is complicated, as for the O1s spectra, due to the formation of what appears to be background-induced aluminum oxide.[50]

To determine in more detail if Al atoms penetrate to the S/Au interface as well as interact with the surface OCH_3 groups, a set of variable takeoff angle spectra was obtained at $\theta_{Al} = 5.3$. The results are shown in Figure 11, where the selected core-level peak areas are plotted as the area ratio to the Au 4f peak at a given takeoff angle normalized to the same ratio at the 15° grazing angle $[(I/I_{Au4f})_\theta/(I/I_{Au4f})_{15}]$. The data can be understood in a qualitative way on the simple basis that at 15° the photoelectrons sampled have a much higher fraction coming from atoms at the ambient surface as compared to the fraction at higher angles where the sampling shifts toward the deeper regions of the sample. The plot shows three calibration curves (dashed lines): O 1s and C 1s data for the ambient surface OCH_3 group layer and C 1s for the alkyl chain $-CH_2-$ group layer

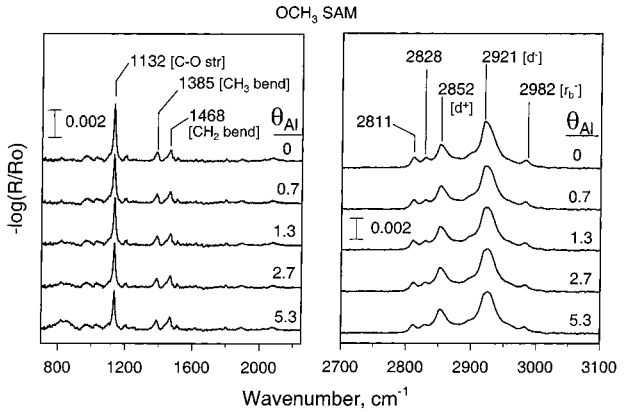

Figure 12. Low- and high-frequency region IRS spectra of the OCH_3 SAM as a function of Al coverage. The inset shows a plot of the C−O stretching mode integrated intensity as a function of the Al coverage.

(∼17 Å thick). As expected for an ambient surface layer, the C 1s and O 1s curves for the $-OCH_3$ group drop together identically with increasing angle and exhibit the fastest falloff of all the data. The curve for the $-CH_2-$ signal drops off much more slowly, in accordance with the carbon atoms being distributed in a region spanning the Au surface and the ambient surface. The data for the Al 2p are divided into the signal for the metallic (zerovalent) signal and the signal attributed to the nonmetallic Al−S and/or Al−O species.[51] Note that the Al 2p metallic peak closely follows the dropoff with angle shown by the surface OCH_3 data. This establishes that metallic Al is deposited primarily at the ambient/SAM surface. In contrast, the Al−O/Al−S peaks closely follow the alkyl chain ($-CH_2-$) layer falloff. This implies that these species are found distributed both at the surface and at the Au/S interface and is consistent with the formation of an Al−S species at the Au surface for Al atoms that penetrate the SAM and some formation of Al−O species at the ambient surface. We note that these conclusions are to be regarded as somewhat qualitative due to uncertainties in the exact assignments of the Al reaction products at low coverages.[41]

3.3.2. IRS. The IR spectra of the H_3CO-terminated monolayer, before and after Al deposition, are shown in Figure 12. The previously reported peak assignments[29,52,53] of the bare monolayer are summarized here for reference. The 1132, 1392, and 1468 cm^{-1} peaks are assigned as the C−O−C antisymmetric stretch (ν_{C-O}), the $-CH_3$ symmetric deformation (δ_{CH_3}), and the $-CH_2-$ scissor deformation (γ_{CH_2}), respectively. The $-CH_2-$ d^+ and d^- stretches are assigned at 2851 and 2918 cm^{-1}, respectively. The peaks at 2811, 2828, and 2981 cm^{-1} have been assigned to the various stretching modes of the terminal CH_3 group. The features at 2811 and 2828 cm^{-1} are assigned as $-CH_3$ Fermi resonance modes. These data indicate that the starting monolayer is well organized with the chains primarily in all-trans conformations.[29]

The low-frequency region shows that features related to the OCH_3 and the CH_2 groups are only slightly perturbed upon deposition of Al. First, the ν_{C-O} stretch mode at 1132 cm^{-1} decreases in intensity slightly but remains relatively unchanged

(51) The intensities of these peaks were first corrected for the presence of a weak Au5p feature at ∼75 eV.
(52) Ong, T. H.; Davies, P. B.; Bain, C. D. *Langmuir* **1993**, *9*, 1836−1845.
(53) Allan, A.; McKean, D. C.; Perchard, J.-P.; Josien, M.-L. *Spectrochim. Acta* **1971**, *27A*, 1409−1437.

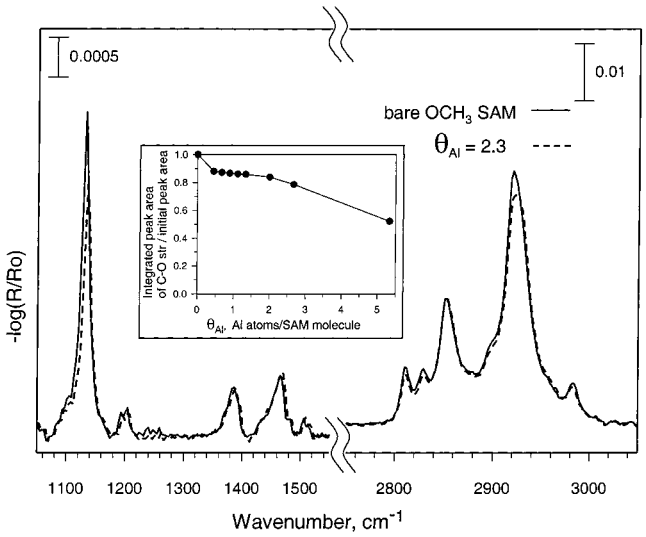

Figure 13. Overlay of the IRS spectra of the OCH_3 SAM before (—) and after (- - -) deposition to a coverage of $\theta_{Al} = 2.3$. Inset: Plot of the fractional integrated intensity of the C−O stretching band of the OCH_3 SAM as a function of Al coverage.

until $\theta_{Al} \approx 2.7$ Al atoms/molecule whereafter the only effect is increasingly rapid intensity attenuation. A more detailed look for $\theta_{Al} = 2.3$ is given in the overlay with the initial bare monolayer spectrum in Figure 13. The C−O stretching mode is observed to shift upward by 4 cm^{-1} with the Al deposition and appears to sharpen. The change in C−O peak area with θ is shown in the inset in the figure. The sharpest change is at $\theta_{Al} \approx 0.5$, whereas thereafter the effects of Al level off until about two Al atoms/OCH_3.

Second, the δ_{CH_3} and γ_{CH_2} features remain essentially unaffected upon deposition of Al. These observations indicate that there is no significant chemical interaction of the OCH_3 group by Al. Furthermore, in contrast to the OH SAM case (see earlier), there is no observation of an Al−O stretch in the spectra, expected at ~855 cm^{-1}. This establishes that no bond cleavage takes place at the methoxy group to form metal-oxide species.

The high-frequency region of the spectrum in Figures 12 and 13 indicates that the d^+ and d^- CH_2 C−H stretches, as well as other bands in the high frequency region, become only slightly perturbed upon deposition of Al. In fact, the only observed shift is with the d^- mode (2921 cm^{-1}) which moves to higher frequency by only ~1 cm^{-1} (see Figure 13). These data establish that the conformations of the alkyl chains are virtually undisturbed by the deposited Al.

4. Discussion

The schematic summary diagram in Figure 1 serves as a convenient general background picture for the discussion. The detailed discussion will be made with reference to the sequence of major mechanistic paths shown below.

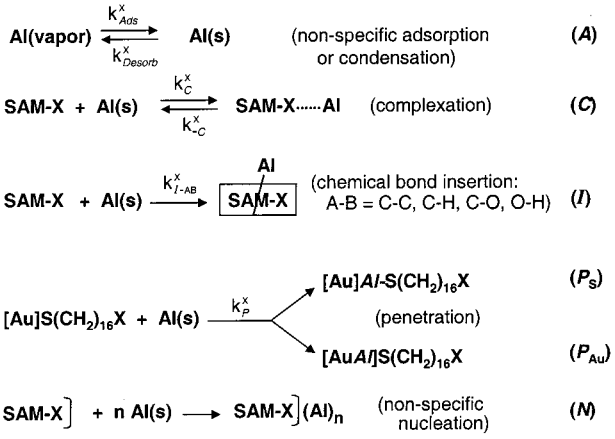

In this mechanism, the fate of the deposited Al atoms is controlled by the competition between local stabilizing interactions (complexation) with a surface group, chemical bond insertion (C−C, C−H, C−O, and O−H, as appropriate), penetration to the interior Au/S interface of the SAM, and nonspecific surface adsorption and film nucleation. For convenience, the monolayer is written as SAM−X, where X is OH or OCH_3 in this study.

The sequence of processes is viewed as starting from adsorption of a deposited Al atom at a random site [Al(s) in process A] on the SAM surface. While this process should be considered as generally reversible, the combination of ToF−SIMS and XPS data in this study does not indicate any desorption of Al atoms from the SAM surfaces.[54] Surface diffusion allows access to locations where processes C, I, and P can occur. The complexation process is written as reversible, characterized by forward and reverse rate constants, k^x_C and k^x_{-C}. The bond insertion and penetration steps are written as irreversible with forward rate constants k^x_{I-AB} and k^x_P, respectively. Penetration is divided into sub paths for adsorption onto a Au lattice site with minimal S atom interaction and complete insertion into a Au−S bond. Nonspecific nucleation (process N) is written purposely to be general and collects together all deposited Al atoms that are not included in the above categories at all stages of Al coverages.

The discussion will proceed by considering the two SAMs in turn, emphasizing the mechanistic aspects of each case. Finally, the overall energetics and structures of species formed by the Al−SAM interactions will be examined.

4.1. HO-Terminated Monolayer—Surface Trapping via OH Chemical Reaction. 4.1.1. Overall Process Sequence. The data indicate that the initial stage of the Al deposition is dominated by insertion of an adsorbed Al atom into an O−H bond (reaction I-OH) to form an O−Al−H species. This implies that $k^{OH}_{I-OH} \gg k^{OH}_P$. Neither C−H and C−C bond reactions nor penetration of Al atoms to the Au/S interface is observed. Following consumption of about one Al atom per group, a premetallic phase of Al nucleates and grows for about two layers until growth of a metallic phase initiates.

4.1.2. O−H Bond Insertion Process. Strong evidence for Al-induced cleavage of the O−H bond is given by the ToF−SIMS and IR data (Figures 3 and 5). In particular, the

(54) There are reported cases of desorption of metal atoms' vapor deposited onto organic substrates, typically observed for cases of noble metals on polymers with very low surface energies (see, for example: Zaporojtchenko, V.; Behnke, K.; Strunskus, T.; Faupel, F. *Surf. Interface Anal.* **2000**, *30*, 439−443. Thran, A.; Kiene, M.; Zaporojtchenko, V.; Faupel, F. *MRS Bull.* **1999**, July, 3). In the case of the OH and OCH_3 SAMs of the present study, desorption does not appear to occur as determined by comparing QCM response with ToF−SIMS and XPS results. Specifically, the ToF−SIMs and XPS signals that reveal the presence of Al monotonically track the QCM coverages, which involve crystals precoated with metal films that give unity sticking coefficients. This is particularly important at low Al coverages where the highest probability of desorption will occur.

observation of a new feature in the IR spectrum at ~1850−1900 cm^{-1}, assigned to an Al−H stretching mode, supports Al insertion into the CO−H bond. These data are fully consistent with the XPS spectra (Figure 4).

The positive shifts (~6 cm^{-1} for the d^- mode) and the broadening of the C−H stretching mode peaks (seen in detail in Figure 6) indicate that significant conformational disordering of the alkyl chains occurs in concert with the O−H insertion. This behavior is consistent with the formation of a reaction product at the HO− terminal group that gives rise to steric crowding with increases in the fraction of *gauche* defects near the SAM surface.

The data indicate ~1:1 Al/OH stoichiometry for the O−H insertion (reaction I-OH). The ToF−SIMS data show the complete loss of mass peaks for clusters containing intact adsorbate by $\theta_{Al} = 1.0$ (±0.15) (Figure 2B). Further, in Figure 3A,B, note the biggest change in the appearance of the Al_2O^+ and $[AlO(CH_2)_6]^-$ peaks occurs by $\theta_{Al} = 1.0$. The XPS data (Figure 4A) show complete loss of the $-O\underline{C}H_3$ C 1s peak by $\theta_{Al} = 1.3$. The IRS data (Figure 5A) show a near cessation of changes in the C−O stretching peak region by $\theta_{Al} \approx 0.7$. Thereafter, a small residual feature remains, shifted slightly to higher frequencies than the original C−O feature. These data suggest that ~15−20% of the OH groups do not undergo Al insertion but are simply perturbed in some subtle way.[55]

4.1.2. Formation of a Premetallic Al Phase at Intermediate Coverages. In general, with increasing Al coverage above $\theta_{Al} \approx 1.0$, no further reactions of the −OH group appear to occur. The Al 2p XPS data show (Figure 4) that metallic overlayers finally form at $\theta_{Al} \gtrsim 5.3$, while for $\theta_{Al} \lesssim 2.7$, or slightly higher, a positive valence or otherwise nonmetallic phase forms. A similar nonmetallic aluminum-organic phase was observed prior to the metallic one in previous studies of the HO_2C- and H_3CO_2C-terminated SAMs. In the present case, after cessation of reaction I-OH, the next about two Al atoms continue to form nonmetallic products. It is in this coverage regime that the 850 cm^{-1} peak assigned to the Al−O IR stretching mode begins to grow in intensity (Figure 5). Note that the intensity growth appears very nonlinear with coverage and continues on into the metallic Al region ($\theta_{Al} \approx 5$), while little change is seen in the band shape and peak maximum. This observation suggests that there is reorientation of the initially formed Al−O bond in a direction normal to the metal surface, but in the absence of additional characterization of the nonmetallic aluminum-organometallic phase(s), the underlying reason for the behavior of the Al−O feature remains unclear.

Scheme 1

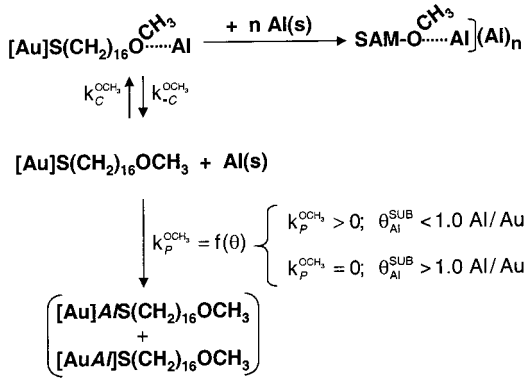

4.2. H_3CO-Terminated Monolayer—Partitioning between Overlayer Film Nucleation and SAM Penetration. 4.2.1. Overall Process Sequence. In complete contrast to the HO-terminated monolayer system, for which bond insertion at the terminal group dominates, the data for the H_3OC-terminated SAM show that the Al atoms exclusively partition between overlayer film nucleation and penetration to the Au/S interface (processes N and P) with no chemical bond breaking. The absence of Al insertion into the OCH_3 group is directly supported by the nearly constant character of the C−O stretching mode at 1132 cm^{-1} in the IRS spectra (Figure 12). Other data are fully consistent with the lack of any chemical reactions with C−H, C−O, and C−C bonds. The lack of a rapid, irreversible insertion reaction of the deposited Al atoms at the SAM surface opens the penetration pathway.

The degree of partitioning between nucleation and penetration is controlled by the strength of stabilization of adsorbed Al atoms at the surface via localized Al···OCH_3 complexation (process C-OCH; with associated rate constants, $k_C^{OCH_3}$ and $k_{-C}^{OCH_3}$). Stabilization reduces access to the penetration channel by reducing surface mobility and enhances overlayer nucleation by maintaining a higher surface Al atom population. With continued Al deposition, the penetration process eventually closes, while overlayer metallic film growth continues.

The essence of the overall mechanism is summarized in Scheme 1.

4.2.2. SAM Penetration versus Overlayer Nucleation—Comparison with Previous Results of a H_3C-Terminated SAM. In both our previously studied case of a H_3C-terminated SAM[26] and the present case of the H_3OC-terminated one, the data show that Al penetrates to the S/Au interface to form a smooth, uniform interfacial adlayer, leaving the chain conformational ordering virtually unperturbed. There is an important difference between the two cases, however. For the OCH_3 SAM, the ToF−SIMS data show that the mixed $Al_XAu_YS_Z^-$ cluster ion peaks, which signal diffusion of Al to the Au/S interface, continue to increase even up to $\theta_{Al} \approx 12.2$ (Figure 8B,C). In contrast, for the CH_3 case, they stop at $\theta_{Al} \approx 2.7$, signaling the

(55) One possible explanation for the appearance of the second Al−OH weak interaction mode is that each event of reaction 1 produces an organoaluminum surface species that occupies more surface area on the SAM than on the original chain terminus. As the deposition proceeds, the formation of adjacent product species will cause disruption of the surface packing and thus eventually could lead to steric screening of the final fraction of unreacted OH groups with a lowered probability of reaction 1. This explanation, however, does not seem likely since in the case of Al atoms deposited on a H_3CO_2C-terminated SAM, the reaction stoichiometry for reaction of the terminal group was very close to 1:1. A second possibility for incomplete reaction is that Al reactivity depends on the H-bonding state of the OH group. It is known that a major fraction of the terminal OH groups in these types of SAMs is H-bonded to neighbors [Atre, S. V.; Liedberg, B.; Allara, D. L. *Langmuir* **1995**, *11*, 3882−3893]. Thus it is possible that the small fraction of nonbonded OH groups could be unreactive towards Al. Approximating the OH groups as being positioned on a ($\sqrt{3} \times \sqrt{3}$) hexagonal lattice with H-bonding in pairs, then ~14% of the groups would be isolated, and thus unreactive with Al. While this fraction is close to what the data suggest, the weak reactivity of the isolated OH groups seems unlikely given the highly favorable thermodynamics for formation of Al−O and Al−H bonds [Chen, J. G.; Basu, P.; Ng, L.; Yates, J. T., Jr. *Surf. Sci.* **1988**, *194*, 397−418. Rogers, J. W., Jr.; White, J. M. *J. Vac. Sci. Technol.* **1979**, *16*, 485−488. Rogers, J. W., Jr.; Hance, R. L.; White, J. M. *Surf. Sci.* **1980**, *100*, 388. Basu, P.; Chen, J. G.; Ng, L.; Colaianni, M. L.; Yates, J. T., Jr. *J. Chem. Phys.* **1988**, *89*, 2406−2411. Waddil, G. D.; Kesmodel, L. L. *Surf. Sci.* **1987**, *182*, L248. Kerkar, M.; Hayden, A. B.; Woodruff, D. P.; Kadadwala, M.; Jones, R. G. *J. Phys.: Condens. Matter* **1992**, *4*, 5043. Stone, F. G. A., West, R., Eds. *Advances in Organometallic Chemistry*; Academic Press: New York, 1996; pp 40−50. Coates, G. E., Green, M. L. H., Wade, K., Eds. *Organometallic Compounds*, 3rd ed.; Methuen & Co.: London, 1967; Vol. 1, pp 295−343], relative to the weak energies of intermolecular H-bonds.

Table 1. Theoretically Calculated Standard Enthalpy Values for the Interaction of an Isolated Al Atom with an Isolated Model Molecule

molecules and Al interaction products	reaction path	$\Delta H°(298)$, kJ/mol	experimentally observed	conclusion/comment
$Al + CH_3CH_2OH$				
-C−Al−OH	I_{CO}	−248 (±9)	no	kinetic barrier too high
-O−Al−H	I_{OH}	−188 (±6)	yes	
Al···O(H)$(CH)_2$−	C_{OH}	−44 (±6)	yes	
$Al + CH_3CH_2CH_3$				
-C−Al−CH_3	I_{CC}	−82 (±7)	no	kinetic barrier too high
-C−Al−H	I_{CH}	−44 (±14)	no	kinetic barrier too high
Al···[$CH_3CH_2CH_3$]	C_{CH}	∼0 (±5)	no	
$Al + CH_3OCH_3$ and $CH_3(CH_2)_4OCH_3$				
-C−Al−OCH_3	I_{CO}	−263 (±8)	no	kinetic barrier too high
-O−Al−CH_3	I_{CO}	−263 (±8)	no	kinetic barrier too high
Al···O$(CH_3)(CH_2)$	C_{OCH_3}	−38 (±5)	yes	

end of penetration. Past this point, Al overlayer growth at the H_3C/vacuum interface proceeds.[26] Other aspects of the ToF−SIMS and XPS data confirm these differences (see sections 3.3.1 and 3.3.2). For example, the XPS data in Figure 11 show that at the intermediate coverage of $\theta_{Al} = 5.3$, the fraction of Al located at the outer surface is dominantly a metallic phase. We analyze these differences in terms of the mechanism in Scheme 1.

First, we set the penetration rate constants for the two SAMs equal, viz., $k_P^{OCH_3} = k_P^{CH_3}$, on the following basis. It was proposed[26] that Al penetration into the CH_3 SAM occurs predominantly via transient defects that arise from thermally activated hopping of the S atoms of the alkanethiolate chains away from their lowest energy positions on the Au surface. Such dynamic fluctuations have been demonstrated theoretically for alkanethiolates on Au(111) and at room temperature are far more rapid than the deposition rates and analysis time in our experiments.[56,57] Because both the CH_3 and the OCH_3 SAMs have virtually identical SAM/Au interfacial structures, chain packing densities, chain organization, and intermolecular interactions, it is reasonable to assume that the transient defect fluctuation processes and their associated penetration rate constants are nearly identical in the two SAMs, viz., $k_P^{OCH_3} \approx k_P^{CH_3}$.

Next we consider the coverage dependence of the penetration processes. It was previously concluded[26] that Al penetration into the CH_3 SAM continues until an ∼1:1 Al:Au adlayer is formed, which for an average Au(111) texture with ∼13 Au atoms/nm^2 would exhibit a substrate saturation coverage $\theta_{Al}^{SUB} \approx 2.8$ Al atoms per molecule. The actual reported saturation coverage of ∼2.7 (∼12.3 Al/nm^2) suggests slightly less than a saturation of 1:1 Al/Au adlayer.[26] Given the near identical SAM structures, we set $\theta_{Al}^{SUB}(OCH_3) = \theta_{Al}^{SUB}(CH_3) \approx 2.7$ Al atoms per molecule as the closure point for the penetration channel in both SAMs.

On the basis of the mechanism in Scheme 1, the difference in the overall values of θ_{Al} required to close the penetration step for different SAMs depends on the competition between the complexation and penetration channels for Al(s). For stabilization of the Al atoms, the associated equilibrium constant for the reaction, written in the direction of complexation of an Al(s), is $K_C^x = K_C^x/K_{-C}^x$. Given that $k_P^{OCH_3} \approx k_P^{CH_3}$ (see above), then to have a comparatively diminished penetration channel in the OCH_3 case, $k_C^{OCH_3} > k_C^{CH_3}$; that is, the OCH_3 group acts as a better Al atom trap or penetration gate than does CH_3.

4.3. Energetics and Structures of the Al + SAM Molecule Interactions. To more firmly establish the basis for the underlying processes that control the course of the Al deposition, quantum theory calculations were carried out for the simple isolated systems of $Al + CH_3CH_2OH$, $CH_3CH_2CH_3$, CH_3OCH_3, and $CH_3(CH_2)_4OCH_3$. Geometry optimization and energies were calculated using a variety of geometrical starting points to facilitate finding the global energy minima of various spatial configurations. The results are summarized in Table 1, where the minimum energies are given in terms of $\Delta H°(298)$. The reported values represent the average of the results for the four basis sets used (see section 2.6), and the errors show the spread in values.

The calculations show that bond insertion is energetically favorable for all the molecular bonds with C−O insertion the most favorable. Because only O−H bond insertion (I-OH) is observed, it appears that the activation barriers for insertion into the other bonds are significantly higher than that for the O−H bond.

Secondary minima at −44 and −38 kJ/mol are found involving primarily a complexation type of interaction between Al and the O atom of the −OH and $-OCH_3$ groups, respectively. In the case of the former, the complex can be viewed as a transient precursor state to a final O−H bond insertion product.[58] In the case of the latter, the data further show that association of an Al with the hydrocarbon unit is thermoneutral thus giving a preference of ∼159 kJ/mol for an Al atom to be located at O rather than C or H atoms of an alkyl ether molecule. Reported theoretical and experimental values for similar systems support the Al···O results. For example, calculations [HF/32-1G, HF/63-1G(d), and MP2/6-31G(d)] for the Al···OH_2 and Al···$O(CH_3)_2$ complexes[24] give stabilization energies of −29 to 33 and −38 kJ/mol, respectively, where the energies include zero-point corrections but not thermal energies. Inclusion of the latter lowers the values by ∼6 kJ/mol. An experimental stabilization energy of −38.4(±2.5) kJ/mol has been reported for the Al···$O(CH_3)_2$ complex.[59]

While the experimental data indicate formation of a simple Al···O(CH_3)R complex, a measure of the interaction strength is difficult to ascertain. For example, the ToF−SIMS and IRS

(56) Bhatia, R.; Garrison, B. J. *Langmuir* **1997**, *13*, 765−769.
(57) Bhatia, R.; Garrison, B. J. *Langmuir* **1997**, *13*, 4038−4043.
(58) Sakai (ref 24) has reported calculations of the transition state barriers of Al insertion in H_2O and $(CH_3)_2O$. The transition state energies are ∼33−46 and ∼88 kJ/mol for H−Al−OH and H_3C−Al−OCH_3 insertion, respectively, relative to the total energy of the isolated reactants. With Al···molecule complexes as precursors, the activation barriers will be raised by the stabilization energy of the corresponding complexes. Sakai notes that for the $(CH_3)_2O$ case the probability of crossing the insertion barrier will be lowered because of orbital overlap effects, making the C−O insertion process, relative to the O−H insertion, less probable than that predicted from energetics alone.
(59) Parnis, M. J.; Mitchell, S. A.; Rayner, D. M.; Hackett, P. A. *J. Phys. Chem.* **1988**, *92*, 3869−3874.

data, as seen in Figures 8 and 13, show only small perturbations of the spectral data with increasing Al deposition, which suggests very weak interaction. In contrast, the XPS C 1s peak associated with the terminal $-CH_2OCH_3$ unit is not observable for $\theta_{Al} \gtrsim 1.3$ (Figure 9A), which suggests that the Al···OCH_3 interaction perturbs the local electron density strongly to cause the binding energy to shift completely into the region of the main C 1s peak. Examination of the structural requirements of the interaction geometry is helpful in exploring these issues. Our theory calculations show that the minimum energy geometry for the Al···O(CH_3)R complex positions the Al atom on the backside of the O atom away from the O−C bonds, as shown below for an isolated $-CH_2-O-CH_3$ unit. Simple examination of the general surface structure of the H_3CO-terminated SAM, as analyzed from space filling models, shows that unfavorable steric interactions at the SAM surface provide a severe molecular reconfiguration barrier to achieving this ideal "backside" configuration, as illustrated in the adjacent cartoon.

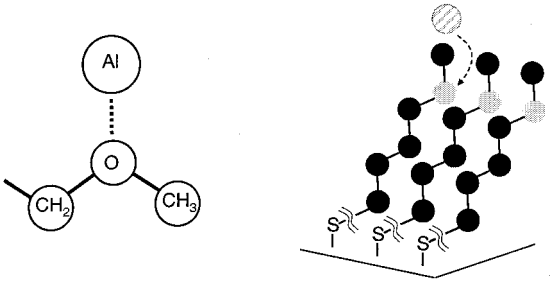

While thermal energies might allow a small fraction of the terminal $-OCH_3$ groups to undergo conformational reconfiguration for favorable Al interaction, it is clear that intermolecular repulsion forces will prevent the vast majority from these conformations. Thus one expects a substantial decrease in the average stabilization energy per Al atom that can be achieved in the SAM relative to the isolated configuration value. This analysis fits qualitatively with the observed behavior of the IR C−O stretching mode (Figures 12 and 13) that shows only a minor shift and almost no change in line shape with deposition of Al. These arguments apply to the OH SAM as well, although the steric blocking should be less with H in place of OCH_3. The weak interaction energies imply a fast dissociation of the Al···O bond in the complex.[60]

Exploring this aspect further, the vibrational mode shifts for the minimum energy Al···O(CH_3)R complex were calculated from theory [B3PW91/6-31G(d,p)]. The results of a detailed analysis[61] for the isolated molecule $CH_3(CH_2)_4OCH_3$, setting different chain and terminal group conformations and examining all variations of modes involving some C−O stretch character, show that the average shift for the C−O frequency is ∼100 cm^{-1} to lower frequencies upon interaction with the Al atom. This shift is much larger, and even in a different direction, than the observed shift, as can be seen in detail in Figure 13. Because this discrepancy is well outside of the inherent errors in the calculations for the levels of theory considered, we conclude that the Al interaction in the SAM is far weaker than the minimum energy configuration predicted from theory, in line with our analysis of the unfavorable steric interactions at the SAM surface. On this basis, we view the interaction between Al and $-OCH_3$ more as a "solvation" rather than a complexation with some directed interaction with a specific geometry. Given the distribution of conformations of the OCH_3 groups at the SAM surface at ambient temperatures, especially in view of the low rotational barriers around an alkyl C−O bond, relative to an alkyl C−C bond, one can expect a wide distribution of geometric configurations of Al relative to the surface atoms of the SAM, analogous to a quasi-isotropic, weakly solvating layer acting on average by mean-field interactions. We note that this picture indicates that approach of an Al atom to the O−CH_3 bond, located at the outermost surface region, would seem not to be sterically blocked. Therefore, we conclude that the lack of Al insertion into this bond, a highly favorable process thermodynamically for isolated model molecules, is due to an activation barrier related to intrinsic electronic effects rather than unfavorable surface configurations.[58] Similarly, we conclude that the observed lack of Al insertion into the C−O bond of the $-CH_2OH$ unit, located just beneath the OH SAM outer surface, arises from intrinsic electronic and atomic reorganization effects as well as unfavorable surface steric effects.

4.3.3. Comparisons of Reactivities of CH_3, OCH_3, CO_2CH_3, OH, and CO_2H Groups. In this and previous reports, we have characterized the reactivities of Al atoms with $-CO_2CH_3$, $-CO_2H$, $-CH_3$, $-OCH_3$, and −OH moieties.[25−27] Because the first two groups can be viewed simplistically as combinations of the latter moieties, along with the C═O unit, it is of interest to check the self-consistency of the chemical reactivities toward Al within the collection of these moieties. The −OH group undergoes bond insertion with Al. Similarly, the main process with $-CO_2H$ appears to be O−H insertion.[27] Neither the $-OCH_3$ nor the $-CH_3$ group is degraded by Al. In the case of the CO_2CH_3 group, the OCH_3 moiety remains intact, consistent with the previous observation, while the C═O bond is completely degraded.[25,26] Overall it appears that while C═O bond attack is favorable relative to C−O, C−C, and C−H bonds, in the presence of an O−H moiety, such as in the CO_2H group, the C═O bond is less reactive than O−H. These comparisons are meant to serve only as a qualitative guide. More detailed bond reactivity correlations will require an expanded set of molecular groups and careful analysis of experimental data.

5. Conclusions and Future Work

The combination of the experimental data and theory calculations shows that the main difference between the interaction of deposited Al atoms with an HO- and a H_3CO-terminated hexadecanthiolate SAM on Au is that the OH group acts as an efficient chemical trap for deposited Al atoms, preventing penetration of the Al into the SAM matrix, while the OCH_3 group provides only very weak stabilization of the Al atoms, analogous to solvation, thereby allowing Al penetration to compete with overlayer film nucleation.

In the case of the OH SAM, while chemical reaction of Al with the OH groups is the dominant channel up to $\theta_{Al} \approx 1$, the reaction appears to cease, regardless of the Al coverage, before

(60) The steric lowering of the ∼40 kJ/mol complex stabilization energies to values approaching several kT in combination with activation barriers for insertion of ∼42−84 kJ/mol sets, $k^{OH}_{I-O-H} < k^{OH}_{-C}$ and $k^{OCH_3}_{IC-O} \ll k^{OCH_3}_{-C}$, suggests that complexation could approach being a rapid preequilibrium step.

(61) The details of more extensive calculations and analysis of interactions involving other metals (e.g., Mg) and molecular groups, related to metal atom deposition on SAMs, will be published elsewhere (Reinard, M. D.; Cabarcos, O.; Allara, D. L., manuscript in preparation).

all the OH groups are reacted, suggestive of steric blocking effects. For $1.0 \lesssim \theta_{Al} \lesssim 3-4$, the deposited Al forms a premetallic phase. Thereafter, a metallic overlayer is observed. Experiments using isotopically labeled molecules with vibrational spectroscopy and ultraviolet photoemission spectroscopy would be useful in characterizing the character of the premetallic phases, and such experiments are currently in progress.

In the case of the OCH_3 SAM, the absence of a strong chemical trap at the SAM surface opens a dynamic defect penetration pathway to the SAM/Au interface where a stable Al adlayer can form. The insertion of Al atoms at this interface occurs with no appreciable effect on conformation or tilt angle of the monolayer indicating the formation of a uniform adlayer. Comparison with the previously studied case of a H_3C-terminated SAM, for which the adlayer is shown to be complete by $\theta_{Al} \approx 2.7$ Al atoms/molecule (or ~1:1 Al/Au for a Au(111) surface) with a crossover thereafter to overlayer growth, leads to the conclusion that the observed continuation of Al penetration well past this coverage for the OCH_3 SAM is due to a stronger surface stabilization of Al atoms by OCH_3 than CH_3. A combination of quantum theory calculations and molecular conformation arguments shows that the Al interactions with the surface atoms in the OCH_3 SAM suffer strong steric effects that reduce the average interaction energy from the ideal value of ~25 kJ/mol. The resulting weakened interactions can be considered axially isotropic, analogous to a weak surface solvation operating via mean field interactions, as opposed to directed ones. This type of information is a useful complement to a variety of gas-phase studies of the solvation interactions of metal atoms and clusters with solvent molecules. In this regard, one would expect a correlation between the interaction SAM/metal interaction mechanism and the morphology of the nucleating overlayer, for example, the "wetting" of the metal across the surface and the sizes of clusters formed. Variable temperature, in situ atomic force microscopy would be useful in characterizing these aspects, and such experiments are underway in our laboratories.

Temperature-dependence studies, coupled with theory and simulation studies, should prove very useful in determining the detailed energetics of this system. Such studies, involving both Al and related metal atoms (e.g., Mg), are in progress.

Overall, these studies reveal substantial details of the interfaces that form from vapor deposition of Al atoms on organic surfaces and provide a better understanding of the specific mechanisms of chemical attack on the previously studied H_3C-, H_3CO_2C-, and HO_2C-terminated SAMs. The work makes clear the myriad of attainable chemical variations possible with metallized organic systems and provides a basis for designing and understanding the properties of many types of Al metallized organic structures, particularly in applications such as novel molecule-based electronic devices where extremely fine control of the contact interfaces is critical.

Acknowledgment. The authors acknowledge financial support from the Office of Naval Research, the National Science Foundation, and the National Institutes of Health. The authors also acknowledge Alfred Miller and the XPS facility at Lehigh University for their valuable cooperation in the XPS experiments.

Supporting Information Available: Preparation and characterization data for ^{18}O-labeled compounds and ToF−SIMS data for initial SAMs (PDF). This material is available free of charge via the Internet at http://pubs.acs.org.

JA0123453